eISSN: 2976-1190

Journal of Engineering and Sciences

Vol. 3 Issue 1 May 30, 2024/ ***DOI:*** *https://doi.org/10.3126/jes2.v3i1.66240*

Journal homepage: Journal of Engineering and Sciences (nepjol.info)

Publisher: Research Management Cell, Pashchimanchal Campus, Lamachour, Pokhara

Multi-Directional Wind Turbine with Combined Savonius and Darieus Rotors: A Comparative Performance Analysis

Swarnim Duwadi[1], Pawan Khanal[1], Abhishek Pandey[1]*

[1] *Department of Automobile and Mechanical Engineering, IOE Thapathali Campus, Tribhuvan University, Nepal*

(Manuscript Received 09/03/2024; Revised 16/05/2024; Accepted 19/05/2024)

Abstract

This study presents a comprehensive investigation into five distinct combinations of wind turbine configurations, each integrating Savonius and Darrieus rotors on a single shaft. The studied configurations include Single Stage Savonius and H-Darrieus, Two-Stage Savonius and D-Darrieus, Two-Stage Savonius and H-Darrieus, Helical Darrieus and Two-Stage Savonius, and Two-Stage Savonius and H-Darrieus in series. Our research uses Computational Fluid Dynamics (CFD) simulations conducted using ANSYS Fluent to meticulously analyze and optimize these turbine designs. Through rigorous computational modeling and flow analysis, we aim to elucidate the performance characteristics, including torque generation, torque nature, flow time, and power output, for each configuration. Following thorough comparison, our findings highlight the double-stage Savonius and D Darrieus turbine as exhibiting superior performance attributes. This research contributes valuable insights into the advancement of multi-directional wind turbine technology, facilitating enhanced energy harnessing from varying wind conditions.

Keywords: Savonius; Darrieus; Multidirectional wind turbine; CFD; Flow analysis

1. Introduction

Wind turbines are broadly categorized as either horizontal-axis wind turbines (HAWTs) or vertical-axis wind turbines (VAWTs). HAWTs, which are the most used type, feature aerodynamic blades, or airfoils, and can be mounted on a rotor with either an upwind or downwind position. These turbines usually have two or three blades that operate at high speeds at the blade tip. They have variable blade pitch, which enables them to capture the wind at the optimal angle for maximum energy generation. HAWTs are known for their high efficiency, as their blades always remain perpendicular to the wind, and generate electricity throughout their rotation. They can operate at high wind speeds due to their tall tower bases. Upwind rotor machines require a yaw mechanism to orient them to the wind, while downwind rotor machines have coned blades that self-align [1].

Despite their advantages, HAWTs have several disadvantages. They feature tall masts and massive blades, making them challenging to construct, transport, and install. The towers must be sturdy enough to hold the massive blades, gearbox, and generator. In addition, HAWTs require a yaw control system, which can be laborious to maintain, to turn the blades in the direction of the wind speed. HAWTs are also highly visible across large areas due to their great height and structure, which can distort the landscape's natural beauty. Moreover, turbulence occurs when a blade passes into the wind shadow of a tower, causing structural damage and wear and tear. Finally, HAWTs are prone to failure due to cyclic loads and vibrations[2].

In contrast, VAWTs provide a viable solution for these regions due to their ability to operate at lower cut-in wind speeds, their lack of yawing requirement, and their lower structural support needs. VAWTs have several advantages over HAWTs. First, VAWTs do not require a sturdy supporting tower, as the generator, gearbox, and other components are situated on the ground. This design allows them to generate power in any direction, regardless of the wind's direction. Second, VAWTs have lower manufacturing and maintenance costs compared to HAWTs, making them a more cost-effective solution. Third, VAWTs do not require yaw and pitch mechanisms, which means they do not need to be oriented in the direction of the wind to be efficient. Fourth, VAWTs are lightweight and easy to install, making

*Corresponding author. Tel.: +977- 9843214826,
E-mail address: pandey.abhishek@email.com

them ideal for use in urban areas where space is limited. Finally, VAWTs are well-suited to extreme weather conditions, such as those found in mountainous regions, where they can provide electricity to mountain huts and other remote locations [1], [2], [3], [4].

While VAWTs offer several advantages over HAWTs, they also have some disadvantages to consider. One limitation is that their low rotational speed may lead to reduced energy output. Moreover, VAWTs require a higher wind power density to operate efficiently, and their installation and maintenance costs are generally higher than those of HAWTs. It is essential to weigh the pros and cons of both types of turbines and consider the specific requirements of each project before deciding which type of turbine to use. This study compares the performance of various combinations of HAWTs and VAWTs to capitalize on their advantages and lessen their disadvantages [5], [6].

The Darrieus-Savonius rotor combines the benefits of the Savonius rotor, such as strong starting torque, with the benefits of the Darrieus rotor, such as a high-power coefficient, in a single rotor. A vertical axis wind rotor of the combined Savonius-Darrieus type has various advantages over separate Savonius or Darrieus wind rotors, including higher efficiency than the Savonius rotor and higher starting torque than the Darrieus rotor. The combined Darrieus-Savonius wind turbine is designed to improve the Darrieus rotor's low-speed performance. The Savonius buckets are constantly attached to the rotor shaft in a combined turbine, but the Darrieus blades are located far from the shaft and have arm attachments to the shaft. Two rotors are mounted on the same shaft in a simple combined turbine[6].

2. Computational Fluid Dynamics (CFD)

Computational Fluid Dynamics (CFD) is a method that mathematically models fluid flow phenomena and solves them numerically using computers. The solution procedure in Computational Fluid Dynamics (CFD) involves several sequential steps to accurately simulate fluid flow phenomena. Firstly, a computational domain is defined, encompassing the area where fluid flow is being studied. This domain is then discretized into a grid or mesh, consisting of small elements known as cells. In two-dimensional domains, cells represent areas, while in three-dimensional domains, they represent volumes. The quality of the grid significantly impacts the accuracy of the CFD solution, so careful attention is paid to ensure high-quality grid generation. Secondly, boundary conditions are specified at the edges or faces of the computational domain. These conditions dictate the behavior of the fluid at these boundaries and are essential for accurately representing real-world scenarios. Next, the type of fluid under investigation (such as water, air, or gasoline) and its properties (temperature, density, viscosity, etc.) are defined. Many CFD software packages come equipped with built-in databases for common fluids, simplifying this step. Afterward, numerical parameters and solution algorithms are selected. These parameters and algorithms vary depending on the specific CFD software being used and are chosen to ensure an accurate and efficient solution of the governing equations. Once all preliminary settings are established, starting values for flow field variables are specified for each cell within the domain. These initial conditions serve as the starting point for the iterative solution process [7].

The core of the solution procedure involves solving the discretized forms of the governing equations iteratively. Typically, this is done at the center of each cell. Throughout the iterations, the residuals, which measure the deviation of the solution from exact, are monitored. The goal is for these residuals to decrease with each iteration, indicating convergence towards a final solution. Once convergence is achieved, flow field variables such as velocity and pressure are visualized and analyzed graphically. Additionally, custom functions formed by algebraic combinations of these variables can be defined and analyzed. Finally, global properties of the flow field, such as pressure drop, and integral properties, such as forces and moments acting on a body, are calculated from the converged solution. Monitoring these properties along with residuals during the iteration process helps ensure convergence and accuracy [8].

The convergent solution is used to determine integral and global characteristics of the flow field, including pressure drop, forces (lift and drag), and moments acting on a body. This may also be done as the iterations progress in the majority of CFD programs. The global and integral characteristics should stabilize to constant values once a solution has converged; therefore, it is often a good idea to keep an eye on them along with the residuals during the iteration process[9].

The Navier-Stokes equation is the most basic governing equation utilized in the calculation of fluid dynamic problems. It was created in France by Claude Louis Naiver in the first decade of the 1800s, and in the middle of the century, English scientist and physicist Sir George Stokes further improved and modified it. In essence, a Newtonian fluid's viscosity effects are added to by the Naiver-Stoke equation. Numerous single-phase flow issues where fluid flow is present can be solved using these equations. Euler's equation is simplified to create the Navier-Stokes equation. The energy equation, continuity equation, and

momentum equation make up the governing equations [10].

The Navier-Stokes continuity equation is written as:

$$\frac{\partial \rho}{\partial t} + \frac{\partial(\rho u)}{\partial x} + \frac{\partial(\rho v)}{\partial y} + \frac{\partial(w)}{\partial z} = 0 \qquad (1)$$

The above equation is time-independent. This equation is used to explain the conservation of mass concept. The notations used are ρ is density in kg/m^3, t is the time, u is the velocity in the x-direction, v is the velocity in the y-direction, w is the velocity in the z-direction, and the x, y and z the direction coordinates. The momentum equation of the Navier-Stokes is given by following three time-dependent and non-dimensional equations [11].

$$\frac{\partial(\rho u)}{\partial t} + \frac{\partial(\rho u^2)}{\partial x} + \frac{\partial(\rho uv)}{\partial y} + \frac{\partial(\rho uw)}{\partial z} = -\frac{\partial p}{\partial x} + \frac{1}{\mathrm{Re}}\left[\frac{\partial \tau_{xx}}{\partial x} + \frac{\partial \tau_{xy}}{\partial y} + \frac{\partial \tau_{xz}}{\partial z}\right] \qquad (2)$$

$$\frac{\partial(\rho v)}{\partial t} + \frac{\partial(\rho uv)}{\partial x} + \frac{\partial(\rho v^2)}{\partial y} + \frac{\partial(\rho vw)}{\partial z} = -\frac{\partial p}{\partial y} + \frac{1}{\mathrm{Re}}\left[\frac{\partial \tau_{xy}}{\partial x} + \frac{\partial \tau_{yy}}{\partial y} + \frac{\partial \tau_{yz}}{\partial z}\right] \qquad (3)$$

$$\frac{\partial(\rho w)}{\partial t} + \frac{\partial(\rho uw)}{\partial x} + \frac{\partial(\rho vw)}{\partial y} + \frac{\partial(\rho w^2)}{\partial z} = -\frac{\partial p}{\partial z} + \frac{1}{Re}\left[\frac{\partial \tau_{xz}}{\partial x} + \frac{\partial \tau_{yz}}{\partial y} + \frac{\partial \tau_{zz}}{\partial z}\right] \qquad (4)$$

3. Literature Review

The efficiency of wind turbines depends on factors such as wind speed, air density, and the size of the blades, all of which have a significant impact on the turbine's capacity to produce power.

The first horizontal-axis wind turbines (HAWTs) with aerodynamic blades were designed in 1891[12]. Since then, HAWTs have become more popular, with over 300,000 units installed worldwide in more than 100 countries, generating over 300 GW of power. It wasn't until 1922 that the first practical VAWTs were developed. French engineer Sigurd J. Savonius invented a drag-based VAWT with rounded blades that collected wind in a cup and used the drag to operate the turbine [13]. While they were less efficient due to their slow rotational speed, they were dependable and produced significant torque at low wind speeds. In 1931, Georges Jean Marie Darrieus invented a VAWT with vertical airfoils, which became the most important VAWT design [14]. During the 1920s and 1930s, several common VAWT designs were proposed and explored, including the Savonius rotor, Madaras rotor, and the Darrieus VAWT. At the time, windmills were widely used across Europe for milling grain and pumping water [15]. Eole, a Darrieus turbine in Canada with a capacity of 2.5 MW, was the largest ever constructed. While the power sector is still dominated by HAWTs, recent advancements in airfoil design, blade geometry, and materials have renewed interest in VAWTs. VAWTs have also been developed for low-speed wind caused by moving vehicles, such as cars and trains. The concept of Darrieus VAWTs was reintroduced in the 1960s by researchers Peter South, Raj Rangi, and Jack Templin, who worked at the National Research Council of Canada. This French concept, which had largely gone unnoticed until then, was brought back to attention by the researchers, and they have since contributed to the development of VAWT technology [16].

In 2006, Mark Oberholzer introduced the concept of generating electricity from wind produced by passing vehicles on highways [17]. He proposed to incorporate turbines into the barriers between highway lanes. Since then, several research papers have been published worldwide to assess the feasibility of the idea, indicating the potential for low-speed turbines.

In a study conducted in 2017, the objective was to design and fabricate a wind turbine capable of powering small street lights. The research focused on the environmental conditions and construction feasibility in Abu Dhabi, UAE. The Sea Hawk design, a type of vertical axis wind turbine, was selected for its compatibility with the region's wind speeds and ease of construction. A three-phase AC generator was utilized due to its widespread availability in the area, while a 12V battery served as an energy storage solution. A charge controller was employed to regulate the flow of charge into the battery and to control turbine rotation when the battery reached full capacity. Turbine blades were crafted from foam board according to the NACA 0018 airfoil shape, with a chord length of 15cm, and the connecting shaft was made of stainless steel. The study encompassed structural analysis, computational fluid dynamics (CFD) analysis, and various calculations to optimize performance. Testing revealed that at a wind speed of 6.4 m/s, the turbine produced a maximum voltage of 2.4V and rotated at a speed of 60.3 rpm[18].

In 2013, Ali studied the performance of Savonius wind turbines with two and three blades at low wind speeds. The study found that the two-blade Savonius wind turbine had more power coefficient than the three-blade turbine evaluated at a similar testing condition [19].

Bankar and Dhote in 2015 designed and tested

savonius vertical axis wind turbine finding that the setup could generate enough power to fulfil at least 10% of energy consumption. Moreover, to enhance the number of rpm in low wind speed conditions, a multi-stage generator with a double generation concept, employing the same size rotor and gear arrangement, can be utilized. This turbine is typically suitable for heights of 8 to 10 meters above ground level since wind velocity at ground level is generally low [20]. A comprehensive study comparing the advantages and disadvantages of two types of wind turbines, namely vertical axis wind turbines (VAWTs) and horizontal axis wind turbines (HAWTs) was conducted by Saad and Asmuin in 2014. The study evaluated the applications of both types of turbines, highlighting the importance of considering location and wind speed in selecting the appropriate design. The study revealed that HAWTs with propeller blades are the most used type and can achieve an impressive 60% efficiency, making them a popular choice for generating electricity from wind power [21].

In 2021, a study delved into Saudi Arabia's Vision 2030 and its implications for renewable energy integration. The research focused on an innovative off-grid application involving a vertical axis wind turbine (VAWT) to power a highway street lamp. VAWTs were chosen for their ease of installation, adaptability to varying wind speeds, and resilience to harsh weather conditions, aligning with the Kingdom's renewable energy goals. Utilizing MATLAB for circuit design and battery state of charge (SOC) analysis under different load scenarios, alongside an Arduino-based weather station and automated street lamp control, the study aimed to optimize energy efficiency. Field tests on highways confirmed the feasibility of harnessing wind power for sustainable street lighting[22]. Similarly, Vitala and Hassan's study in 2014 showed that wind energy could be harnessed from roadways most efficiently at a height of 120 cm. The study also emphasized the importance of considering the aspect ratio in the VAWT's design [23].

In a study conducted by S. Bruca, R. Lanzafame, and M. Messina, they investigated the relationship between the aspect ratio and the performance of turbines. The study revealed that turbines with a smaller aspect ratio had a higher power coefficient and better in-service stability due to the thicker blade structure [24]. These models relied mainly on drag components with little to no lift, even at low speeds. In 2017, undergraduate research students from the Department of Automobile and Mechanical Engineering at IOE, TU designed a prototype of the vertical-axis wind turbine. However, the project turned out to be excessively expensive compared to other renewable energy sources [25].

Incorporating a Savonius rotor into a hybrid Vertical Axis Wind Turbine (VAWT) enhances its ability to start on its own, but it also creates vortices that lead to fluctuating loads on the Darrieus blades. This research seeks to identify and analyze the airflow patterns surrounding the hybrid VAWT and establish a connection with the variations in force experienced by the Darrieus blades during a single rotation [26]. It is also important to note that the recent development of building integrated wind turbines has opened the space for energy generation in urban areas. Many computational analyses are conducted in two dimensions confining researchers to a setup where the Savonius rotor is positioned between the Darrieus blades. To explore alternative arrangements, such as placing the Savonius rotor either above or below the Darrieus rotor, three-dimensional computational or experimental investigations are essential [27], [28], [29]. This study aims to computationally compare the power generation performance of multi-directional wind turbines with different rotor settings.

4. Turbine Design

4.1 Assumptions and Design Parameters

To ensure portability and easy installation on highways or rooftops, a turbine height of 0.75 m was chosen, along with an outer rotor radius of the same length to achieve an aspect ratio of 1. However, due to design complications, the D-Darrieus rotor's aspect ratio was set to 0.667. This lower aspect ratio offers advantages such as increased power coefficient and stability. Although an aspect ratio of around 1 was more popular in past works, an aspect ratio of 1 provides design simplicity and is practical for applications. To maintain symmetry, the inner Savonius rotor also has an aspect ratio of 1. The combined turbine design follows the standard 2-blade Savonius and 3-blade Darrieus configuration. The chord length for the H-Darrieus rotor was set at 24% of the rotor height, while a small shaft with a diameter of 30mm was chosen. Helical blades were designed with a height and revolution of 0.75m and 0.5, respectively.

4.2 Single Stage Savonius and H-Darrieus

The turbine comprises an inner single-stage Savonius rotor and an outer Darrieus rotor, with both turbines having an aspect ratio of 1 as shown in Figure 1. The H-Darrieus rotor operates using the lift force generated by the airfoil shape, while the Savonius stage works based on the drag force created by the air. Initially, the Savonius stage provides the necessary starting torque.

Once the threshold RPM is reached, the Darrieus stage takes over, and the entire turbine rotates as a single unit.

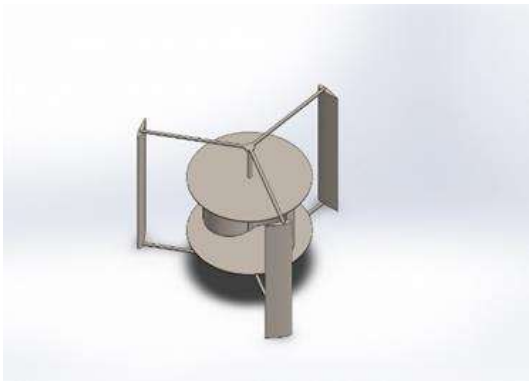

Figure 1: Single Stage Savonius and H -Darrieus

4.3 Two-Stage Savonius and D-Darrieus

Designing vertical axis turbine blades is a challenging task, as the constantly changing forces resulting from the varying angle of attack can lead to torque ripple, vibrations, and noise, and can put significant stress on the blade structure and other turbine components. The loading can be compared to fatigue loading, and since the optimal angle of attack occurs at just one location, it can lead to reduced torque and compromised efficiency. To address issues related to fatigue loading, designers can consider using eggbeater-shaped blades for the Darrieus turbine as shown in Figure 2.

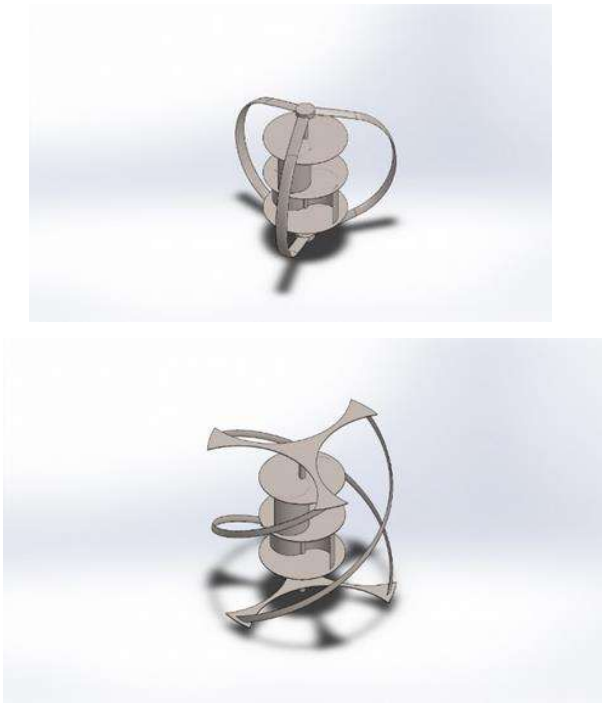

Figure 2: Two-Stage Savonius and D-Darrieus

This blade design arrangement allows the blades to be primarily loaded in tension, which is better suited for certain materials that perform better in tension than in compression. This design option can help increase the lifespan of the turbine blades, reducing maintenance costs and improving the overall efficiency of the turbine.

4.4 Two-Stage Savonius and H-Darrieus

The turbine is composed of an inner two-stage Savonius rotor and an outer Darrieus rotor, with both turbines having an aspect ratio of 1 as depicted in Figure 3. The H-Darrieus rotor generates lift force across the airfoil shape, while the Savonius stage operates on the drag force created by the air. The Savonius stage provides the necessary starting torque, and once the threshold rpm is reached, the Darrieus stage takes over and the entire turbine rotates as a single unit. The two Savonius stages are oriented at a 90° angle to each other, providing better torque stability than a single-stage setup.

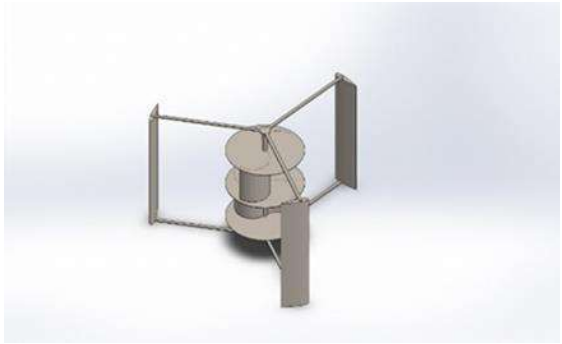

Figure 3: Two-Stage Savonius and H-Darrieus

4.5 Helical Darrieus and two stage Savonius

Reducing output variability in wind turbines can be achieved through different methods. One approach is to add more blades, which can decrease the probability of all blades stalling simultaneously and lead to a smoother output. However, beyond a certain point, adding more blades may become impractical and expensive. An alternative solution is to use helical blades, which have a continuous curve along their length and distribute the load evenly across the blade's entire surface. Helical blades produce a more stable torque than straight blades, thereby reducing output fluctuation. However, designing and manufacturing complex helical blades can present challenges. Figure 4 shows the helical Darrieus and two-stage Savonius rotor design.

Figure 4: Helical Darrieus and two stage Savonius

4.6 Two-Stage Savonius and H-Darrieus in series

The design is similar to the previous design except that the two-stage savonius rotor is placed end-to-end instead of placing it inside the outer h-darrieus rotor as shown in Figure 5.

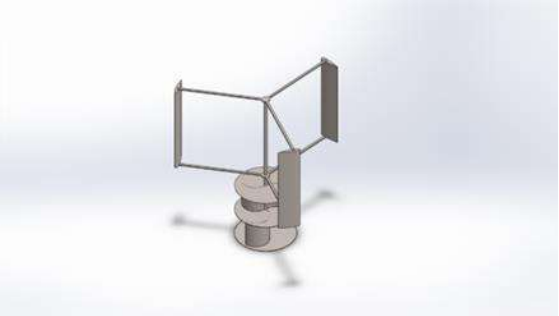

Figure 5: Two-Stage Savonius and H-Darrieus in series

5. Methodology:

The methodology employed in this study involved a systematic approach to design, simulate, and analyze multi-directional wind turbine configurations using Computational Fluid Dynamics (CFD) techniques.

Firstly, the turbine geometry was created using Solidworks. This involved designing the turbine components, including Savonius rotors and Darrieus blades, in various configurations to explore different turbine setups.

Subsequently, Boolean operations were performed to subtract the turbine geometry from the surrounding enclosure, creating a computational domain representing the fluid flow region around the turbine. This step ensured the accurate representation of the rotating turbine components within the simulation.

Meshing, a critical aspect of CFD simulations, was then carried out to discretize the computational domain into smaller elements. Mesh quality, including measures such as orthogonal and skewness qualities, was carefully evaluated to optimize computational efficiency and accuracy. The meshing of 3D models was done with three different levels of meshes. A mesh independence test was conducted using outlet pressure as a key parameter of interest for models with different numbers of meshes. The medium number of meshes with 2757888 elements had less than 3% variation in the outlet pressure with the model with finer mesh. This confirmed that medium coarse mesh was optimal for analysis.

Once the mesh was generated, the Fluent setup was established. Boundary conditions, domain setups, and interfaces were defined to accurately capture the physics of fluid flow around the turbine. Two simulation setups, dynamic mesh and sliding mesh with mesh motion in transient analysis, were utilized to simulate turbine rotation effectively.

For each run, boundary conditions must be given, and the nature of the solution and accuracy are dependent on how these criteria are described. The velocity at inlet 5m/s and static pressure at outflow are the boundary conditions used in this analysis. The turbine's rotational speed is set to 150 rpm. Turbulence is a challenging part that has yet to be fully understood or refined, and there is no ideal model available, but it is essential in practically all engineering fluid flow simulations to forecast how turbulent fluctuations will affect the flow. Turbulence is a dominant phenomenon, which means that when it exists, it has a significant impact on other phenomena. As a result, it's crucial to model it as precisely as possible. Because each model has advantages and disadvantages, it is critical to select the turbulence model that is most suited to the project. The k-epsilon realizable model with wall treatment was employed as the turbulence model.

Table 1: Time step selection

Total number of time steps	500
Time step size	0.001
Maximum iterations per time step	20
Total number of iterations	10000

Solver configuration was tailored to the nature of the problem, with Fluent solving the partial differential equations governing energy, mass, and momentum conservation using the finite volume method. Multiple simulations were conducted with varying inputs to explore the performance of different turbine configurations across a range of operating conditions. Post-simulation analysis involved determining torque and power output from the turbine, providing crucial insights into its performance characteristics.

Through this comprehensive methodology, we were able to systematically evaluate and compare the performance of various multi-directional wind turbine configurations, providing valuable insights into their suitability for different applications and operating conditions.

Figure 6: Flow diagram showing Methodology

6. Results

Fluid flows naturally from an area of high pressure to an area of low pressure, and this flow is harnessed to produce mechanical energy in a turbine. Specifically, the pressure energy of the fluid is converted to mechanical energy in the turbine, allowing it to rotate and generate power. The process is driven by the difference in pressure between the two areas, with the fluid naturally flowing from high to low pressure to equalize the pressure gradient. Figure 6 shows the pressure contour for double-stage Savonius and H Darrieus. The pressure in the area within the turbine is higher than the pressure outside the turbine.

In the rotating domain of a turbine, the inlet air appears to be propelled by the rotation of the domain itself. This is because the turbine absorbs the kinetic energy of the wind, causing the velocity of the fluid downstream to decrease. The velocity contour of the fluid represents the steady-state velocity field for a given iteration, providing insight into the fluid's flow and behavior in the turbine. This behavior is a result of the fluid's interaction with the turbine's rotating blades, which convert the fluid's kinetic energy into mechanical energy that can be used to generate power.

6.1 Single stage Savonius and H Darrieus

Figure 7 shows the moment vs flow time curve for single-stage Savonius and H Darrieus turbine. It shows that although the moment is periodic it is not uniform, and it has different peaks and troughs during each cycle. The rms moment was obtained to be 0.9177 Nm for a turbine rotating at a speed of 150 rpm. The power was calculated to be 14.416W.

Figure 7: Moment vs. flow time curve for single stage Savonius and H Darrieus

6.2 Double-stage Savonius and D-Darrieus turbine

Figure 7 shows the moment vs flow time curve for two-stage Savonius and D-Darriieus turbines. There is a sudden spike in the moment for these hybrid turbines while the frequency of the periodic cycle is lower. The rms moment was obtained to be 0.2271 Nm for a turbine rotating at the speed of 150 rpm. The power was calculated to be 34.07W.

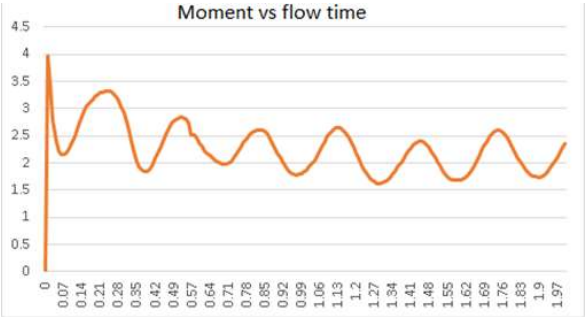

Figure 8: Moment Vs flow time curve for double-stage Savonius and D-Darrieus turbines

6.3 Double stage Savonius and H Darrieus

Figure 6 shows that the moment from the rotor is periodic. It also shows that the variation in the moment is higher and there is a sharp increase and decrease in the moment with time.
The rms moment was obtained to be 2.018 Nm for a turbine rotating at a speed of 150 rpm. The power was calculated to be 31.7013W.

6.4 Two stage Savonius and Helical Darrieus

The moment vs flow time curve shown in Figure 9 of

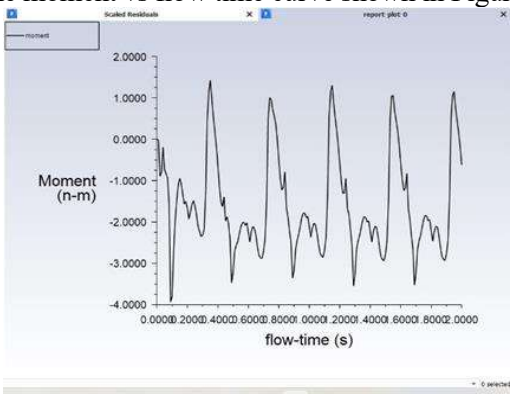

Figure 9: Moment vs. flow time curve of double stage Savonius and H Darrieus

Helical Darrieus and two-stage Savonius is almost similar to the curve for D Darrieus and Savonius turbines.

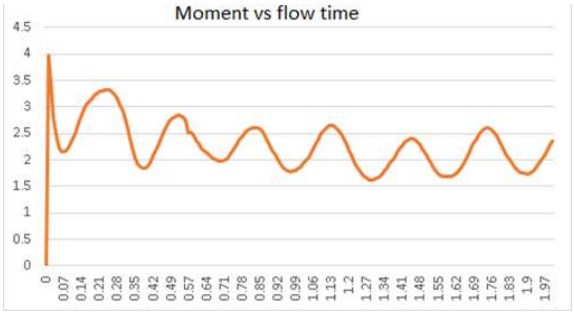

Figure 10: Moment Vs flow time of two stage Savonius and Helical Darrieus

The rms moment obtained was found to be 0.22516 Nm for a turbine rotating at the speed of 150 rpm which is also almost equal to the previous rotor design. The power was calculated to be 33.775W

6.5 Two stage Savonious and H Darrieus in series

It shows that the starting moment is higher and then the moment decreases with flow time stabilizing in a periodic cyclic moment. The rms moment was obtained to be 0.87887 Nm for a turbine rotating at a speed of 150 rpm. The power was calculated to be 13.80W.
The power obtained from various vertical-axis wind turbines is shown in Table 1. It shows that considering only the power generation from different combinations with the same boundary conditions, the two-stage Savonius and D Darrieus turbine is the best hybrid turbine.

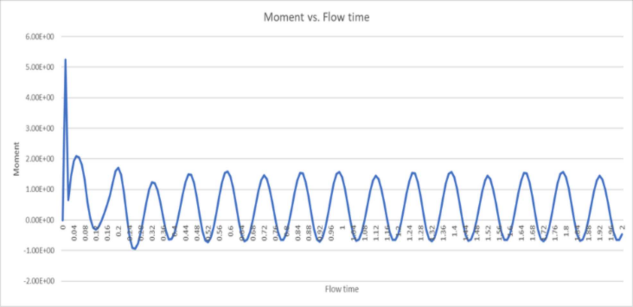

Figure 11: Moment vs. flow time curve for two-stage Savonius and H Darrieus in series

Table 2: Power output of different turbines

Turbine	Power(W)	Speed (rpm)
Single Stage Savonius and H-Darrieus	14.416	150
Two Stage Savonius and D- Darrieus	34.07	150
Two Stage Savonius and H Darrius	14.416	150
Two stage Savonius and Helical Darrieus	13.8	150
Two Stage Savonius and H-Darrieus in Series	33.77	150

7. Conclusion

The comparative performance analysis of various vertical axis wind turbines with identical dimensions revealed that the optimal power output was achieved through a combination of double-stage Savonius and D Darrieus turbines. This combination yielded a power generation of 34.07 Watts at

150 rpm. The Savonius turbine is known for producing high torque at low rotational speed, while the Darrieus turbine produces low torque at high rotational speed. The addition of the Savonius stage had a positive impact on the overall power output, as it generated more torque and hence more power.

The current design was analyzed only in static conditions, without considering any dynamic behavior of the model. Additionally, the turbine's performance is dependent on various parameters, and it would be worthwhile to analyze the design by varying these parameters. And, we recognize the significance of validating our research findings through theory or experiment. We intend to address this concern in the subsequent phase of our study. Specifically, we plan to conduct experimental analysis to complement our Computational Fluid Dynamics (CFD) results. This additional step aims to enhance the reliability and credibility of our findings. We eagerly anticipate incorporating the outcomes of our experimental work into our next paper to further strengthen its scientific rigor.

References

[1] Wagner, H.J. Introduction to wind energy systems, *EPJ Web Conf*, 54 (2013). doi: 10.1051/epjconf/20135401011.

[2] Mansouri, A., El Magri, A., Lajouad, R., El Myasse, I., Younes, E. K. and Giri, F. Wind energy-based conversion topologies and maximum power point tracking: A comprehensive review and analysis, *e-Prime - Advances in Electrical Engineering, Electronics and Energy*, 6 (2023). doi: 10.1016/j.prime.2023.100351.

[3] Spiru, P. and Simona, P. L. Wind energy resource assessment and wind turbine selection analysis for sustainable energy production. *Sci Rep*, 14(1) (2024). doi: 10.1038/s41598-024-61350-6.

[4] Charabi, Y. and Abdul-Wahab, S. Wind turbine performance analysis for energy cost minimization, *Renew Wind Water Sol*, 7(1) (2020). doi: 10.1186/s40807-020-00062-7.

[5] Şağbanşua, L., and Balo, F. Multi-criteria decision making for 1.5 MW wind turbine selection. *Procedia computer science*, *111* (2017) 413-419. doi: 10.1016/j.procs.2017.06.042

[6] Sefidgar, Z., Ahmadi Joneidi, A., and Arabkoohsar, A. A Comprehensive Review on Development and Applications of Cross-Flow Wind Turbines, *Sustainability*, 15(5) (2023) doi: 10.3390/su15054679.

[7] Chung, T.J. *Computational Fluid Dynamics*, Cambridge University Press, 2010 doi: 10.1017/CBO9780511780066.004.

[8] Zong, C., Li, Q., Li, K., Song, X., Chen, D., Li, X., and Wang, X. Computational fluid dynamics analysis and extended adaptive hybrid functions model-based design optimization of an explosion-proof safety valve. *Engineering Applications of Computational Fluid Mechanics*, *16*(1) (2022), 296-315.

[9] Zawawi, M. H., Saleha, A., Salwa, A., Hassan, N. H., Zahari, N. M., Ramli, M. Z., and Muda, Z. C. A review: Fundamentals of computational fluid dynamics (CFD). In *AIP conference proceedings* 2030 (1) (2018). AIP Publishing.

[10] Al-Baali, A. A. G., Farid, M. M., Al-Baali, A. A. G., and Farid, M. M. (2006). Fundamentals of computational fluid dynamics. *Sterilization Of Food In Retort Pouches*, (2006) 33-44.

[11] Fletcher, C. A., & Fletcher, C. A.. Computational Fluid Dynamics: An Introduction. *Computational Techniques for Fluid Dynamics 1: Fundamental and General Techniques*, (1988) 1-16.

[12] Barnard, M. Vertical Axis Wind Turbines: Great In 1890. See: https://cleantechnica.com/2014/04/07/vertical-axis-wind-turbines-great-1890-also-rans-2014/ (last accessed: May 15, 2024.)

[13] Wenehenubun, F., Saputra, A., and Sutanto, H. An experimental study on the performance of Savonius wind turbines related with the number of blades. *Energy procedia*, *68* (2015) 297-304. doi: 10.1016/j.egypro.2015.03.259.

[14] Mohan Kumar, P., Sivalingam, K., Lim, T. C., Ramakrishna, S., and Wei, H. Review on the evolution of Darrieus vertical axis wind turbine: Large wind turbines. *Clean technologies*, *1*(1) (2019) 205-223.

[15] Paraschivoiu, I. *Wind turbine design: with emphasis on Darrieus concept*. Presses inter Polytechnique. (2002).

[16] Möllerström, E., Gipe, P., Beurskens, J., and Ottermo, F. A historical review of vertical axis wind turbines rated 100 kW and above. *Renewable and Sustainable Energy Reviews*, *105* (2019) 1-13.

[17] Poe, C., Filosa, G., Schwarzer, J., Brecher, A., and Millette, K. Alternative uses of highway right-of-way: Accommodating renewable energy technologies and alternative fuel facilities. (2012).

[18] Khan, M., Alavi, M., Mohan, N., Azeez, A., Shanif, A., and Javed, B. Wind Turbine design and fabrication to power streetlights. In *MATEC Web of Conferences*. EDP Sciences. 108 (2017)

[19] Ali, M. H. Experimental comparison study for Savonius wind turbine of two & three blades at low wind speed. *International Journal of Modern Engineering Research (IJMER)*, *3*(5) (2013), 2978-2986.

[20] Dhote, A. and Bankar, V. Design analysis and fabrication of Savonius vertical axis wind turbine. *International Research Journal of Engineering and Technology*, *2*(3) (2015) 2048-2054.

[21] Saad, M. M. M. and Asmuin, N. Comparison of horizontal axis wind turbines and vertical axis wind turbines. *IOSR Journal of Engineering (IOSRJEN)*, *4*(08) (2014) 27-30.

[22] Sundaram, A., Almobasher, L., Al-Eid, M., Bazroon, M., and Abohasson, A. Implementation of a highway wind power generation using a vertical axis wind turbine to automatically power a street lamp. *Wind Engineering*, *45*(5) (2021)1175-1192.

[23] Hassan, M. A. and Vittala, V. Analysis of Highway Wind Energy Potential." See: www.ijert.org (last accessed, May 15. 2024)

[24] Brusca, S., Lanzafame, R., & Messina, M. Design of a vertical-axis wind turbine: how the aspect ratio affects the turbine's performance. *International Journal of Energy and Environmental Engineering*, *5* (2014) 333-340. doi: 10.1007/s40095-014-0129-x.

[25] Bartaula, P. and Shakya, S. R. Design and Numerical Modelling of Vertical Axis Helical Wind Turbine for Highway Application. *Proceedings of 8th IOE Graduate Conference,* (2020).

[26] Pan, J., Ferreira, C. and van Zuijlen, A.. A numerical study on the blade–vortex interaction of a two-dimensional Darrieus–Savonius combined vertical axis wind turbine. *Physics of Fluids*, *35*(12) (2023). doi: 10.1063/5.0174394.

[27] Sarma, J., Jain, S., Mukherjee, P., and Saha, U. K. Hybrid/combined Darrieus–Savonius wind turbines: Erstwhile development and future prognosis. *Journal of Solar Energy Engineering*, *143*(5) (2021). doi: 10.1115/1.4050595.

[28] Liang, X., Fu, S., Ou, B., Wu, C., Chao, C. Y., and Pi, K. A computational study of the effects of the radius ratio and attachment angle on the performance of a Darrieus-Savonius combined wind turbine. *Renewable energy*, *113* (2017)329-334. doi: 10.1016/j.renene.2017.04.071.

[29] Hosseini, A., and Goudarzi, N. Design and CFD study of a hybrid vertical-axis wind turbine by employing a combined Bach-type and H-Darrieus rotor systems. *Energy conversion and management*, *189* (2019) 49-59. doi: 10.1016/j.enconman.2019.03.068.